blood

American Society of Hematology
2021 L Street NW, Suite 900,
Washington, DC 20036
Phone: 202-776-0544 | Fax 202-776-0545
editorial@hematology.org

Less Deformable Erythrocyte Subpopulations Biomechanically Induce Endothelial Inflammation in Sickle Cell Disease

Tracking no: BLD-2024-024608R1

Christina Caruso (Emory University School of Medicine, United States) Xiaopo Cheng (University of Wisconsin-Madison, United States) Marina Michaud (Emory University School of Medicine, United States) Hannah Szafraniec (University of Minnesota, United States) Beena Thomas (Emory University School of Medicine, United States) Meredith Fay (Emory University, United States) Robert Mannino (Georgia Institute of Technology, Emory University, United States) Xiao Zhang (University of Wisconsin-Madison, United States) Yumiko Sakurai (Emory University/Georgia Institute of Technology, United States) Wei Li (Emory University School of Medicine, United States) David Myers (Emory University, United States) Clinton Joiner (Emory University School of Medicine, United States) David Wood (University of Minnesota, United States) Manoj Bhasin (Emory University, United States) Michael Graham (University of Wisconsin-Madison, United States) Wilbur Lam (Emory University School of Medicine, Georgia Institute of Technology, United States)

Abstract:
Sickle cell disease (SCD) is canonically characterized by reduced red blood cell (RBC) deformability leading to microvascular obstruction and inflammation. While the biophysical properties of sickle RBCs are known to influence SCD vasculopathy, the contribution of poor RBC deformability to endothelial dysfunction has yet to be fully explored. Leveraging interrelated in vitro and in silico approaches, we introduce a new paradigm of SCD vasculopathy in which poorly deformable sickle RBCs directly cause endothelial dysfunction via mechanotransduction, where endothelial cells sense and pathophysiologically respond to aberrant physical forces independently of microvascular obstruction, adhesion, or hemolysis. We demonstrate that perfusion of sickle RBCs or pharmacologically-dehydrated healthy RBCs into small venule-sized "endothelialized" microfluidics leads to pathologic physical interactions with endothelial cells that directly induce inflammatory pathways. Using a combination of computational simulations and large venule-sized endothelialized microfluidics, we observed that perfusion of heterogeneous sickle RBC subpopulations of varying deformability, as well as suspensions of dehydrated normal RBCs admixed with normal RBCs leads to aberrant margination of the less-deformable RBC subpopulations towards the vessel walls, causing localized, increased shear stress. Increased wall stress is dependent on the degree of subpopulation heterogeneity and oxygen tension and leads to inflammatory endothelial gene expression via mechanotransductive pathways. Our multifaceted approach demonstrates that the presence of sickle RBCs with reduced deformability leads directly to pathological physical (i.e., direct collisions and/or compressive forces) and shear-mediated interactions with endothelial cells and induces an inflammatory response, thereby elucidating the ubiquity of vascular dysfunction in SCD.

Conflict of interest: No COI declared

COI notes:

Preprint server: No;

Author contributions and disclosures: C.C. and W.A.L. designed the study; X.C. and M.D.G. designed and created computational simulations; H.M.S. and D.K.W. designed and performed rheological microfluidic experiments; B.E.T., M.E.M., and M.B. performed scRNA-seq and its associated statistical analysis; C.C. performed microfluidic experiments; X.Z., M.E.F., R.G.M., Y.S. and D.R.M. designed and performed preliminary experiments; W.L. and C.H.J. developed and helped perform nystatin treatment of RBCs; C.C., X.C., H.M.S., M.E.M., B.E.T. performed data analysis; C.C. wrote the article, all authors reviewed and edited the article; M.B., M.D.G. and W.A.L. oversaw the project.

Non-author contributions and disclosures: No;

Agreement to Share Publication-Related Data and Data Sharing Statement: For original data, please contact wilbur.lam@emory.edu. Accession ID: GSE274340 that's now available on GEO: https://www.ncbi.nlm.nih.gov/geo/query/acc.cgi?acc=GSE274340

Clinical trial registration information (if any):

Title:
Less Deformable Erythrocyte Subpopulations Biomechanically Induce Endothelial Inflammation in Sickle Cell Disease

Short Title:
Erythrocyte-induced Endothelial Inflammation

Authors:
Christina Caruso[1], Xiaopo Cheng[2], Marina E. Michaud[1], Hannah M. Szafraniec[3], Beena E. Thomas[1], Meredith E. Fay[4], Robert G. Mannino[1,4], Xiao Zhang[2], Yumiko Sakurai[4], Wei Li[1], David R. Myers[1,4], Clinton H. Joiner[1], David K. Wood[3], Manoj Bhasin[1,5*], Michael D. Graham[2*], and Wilbur A. Lam[1,4*]

Affiliations:
1. Aflac Cancer and Blood Disorders Center of Children's Healthcare of Atlanta, Department of Pediatrics, Emory University School of Medicine, Atlanta, GA, USA
2. Department of Chemical and Biological Engineering, University of Wisconsin-Madison, Madison, WI, USA
3. Department of Biomedical Engineering, University of Minnesota, Minneapolis, MN, USA
4. Wallace H. Coulter Department of Biomedical Engineering, Georgia Institute of Technology and Emory University, Atlanta, GA, USA
5. Department of Biomedical Informatics, Emory University, Atlanta, GA, USA

***Corresponding Authors:**
Wilbur A. Lam, 412 Emory Children's Center, 2015 Uppergate Drive, Atlanta, GA 30322. Phone: 404-727-7473, Fax: 404-785-6288, Email: wilbur.lam@emory.edu

Michael D. Graham, Engineering Hall Room 3010, 1415 Engineering Drive, Madison, WI 53706. Phone: 608-265-3780, Fax: 608-262-5434, Email: mdgraham@wisc.edu

Manoj Bhasin, 1760 Haygood Drive, Atlanta, GA 30322. Phone: 404-712-9849, Fax: 404-785-6288, Email: manoj.bhasin@emory.edu

For original data, please contact wilbur.lam@emory.edu. Accession ID: GSE274340 that's now available on GEO: https://www.ncbi.nlm.nih.gov/geo/query/acc.cgi?acc=GSE274340

Text word count: 3531
Abstract word count: 244
Figure/table count: 6
Reference count: 38

Key Points

1. Less deformable sickle red cells marginate towards blood vessel walls leading to altered local wall shear stress and endothelial dysfunction
2. Pathological biophysical alterations in sickle red blood cells cause endothelial dysfunction independently from vaso-occlusion and adhesion

Abstract

Sickle cell disease (SCD) is canonically characterized by reduced red blood cell (RBC) deformability leading to microvascular obstruction and inflammation. While the biophysical properties of sickle RBCs are known to influence SCD vasculopathy, the contribution of poor RBC deformability to endothelial dysfunction has yet to be fully explored. Leveraging interrelated *in vitro* and *in silico* approaches, we introduce a new paradigm of SCD vasculopathy in which poorly deformable sickle RBCs directly cause endothelial dysfunction via mechanotransduction, where endothelial cells sense and pathophysiologically respond to aberrant physical forces independently of microvascular obstruction, adhesion, or hemolysis. We demonstrate that perfusion of sickle RBCs or pharmacologically-dehydrated healthy RBCs into small venule-sized "endothelialized" microfluidics leads to pathologic physical interactions with endothelial cells that directly induce inflammatory pathways. Using a combination of computational simulations and large venule-sized endothelialized microfluidics, we observed that perfusion of heterogeneous sickle RBC subpopulations of varying deformability, as well as suspensions of dehydrated normal RBCs admixed with normal RBCs leads to aberrant margination of the less-deformable RBC subpopulations towards the vessel walls, causing localized, increased shear stress. Increased wall stress is dependent on the degree of subpopulation heterogeneity and oxygen tension and leads to inflammatory endothelial gene expression via mechanotransductive pathways. Our multifaceted approach demonstrates that the presence of sickle RBCs with reduced deformability leads directly to pathological physical (i.e., direct collisions and/or compressive forces) and shear-mediated interactions with endothelial cells and induces an inflammatory response, thereby elucidating the ubiquity of vascular dysfunction in SCD.

Introduction

The unique pathology in sickle cell disease (SCD) is caused by a single point mutation in the beta globin gene creating abnormal, sickle hemoglobin, which, upon deoxygenation, polymerizes within the red blood cell (RBC), decreasing its deformability and producing the characteristic "sickled" appearance.[1] The classical paradigm of poorly deformable cells blocking the microcirculation leading to vaso-occlusion and end-organ damage has been expanded to incorporate the pro-adhesive, pro-coagulant, inflammatory vasculopathy associated with endothelial cell (EC) activation driven by intravascular hemolysis, platelet activation, and inflammatory cytokines.[2,3,4,5,6,7] This expanded view of SCD pathophysiology may still be incomplete, as it overlooks a common yet consequential complication of SCD: chronic sickle vasculopathy, including its association with stroke. As SCD vasculopathy, in which ECs are dysfunctional and pro-inflammatory,[8,9,10] occurs even in the highly oxygenated arterial circulation, a new pathophysiologic understanding of SCD is needed. Current theories do not directly link the decreased deformability of sickle RBCs (sRBCs) to endothelial dysfunction, and sRBC-EC biophysical interactions have not been explored.

Cardiovascular bioengineering research has demonstrated that ECs mechanotransduce biophysical cues, such as the shear forces of the hemodynamic microenvironment, into cellular biological signals.[11,12,13] Shear forces can be transduced by ion channels in the EC membrane and various kinases, resulting in the activation of NADPH oxidase and the production of reactive oxygen species (ROS).[14] ROS can further alter EC function via altered

vascular tone by altering nitric oxide (NO) bioavailability or signaling.[15] Moreover, pathological alterations of those forces lead to activation of proinflammatory signals within ECs including upregulation of VCAM-1 and E-selectin and subsequent development of atherosclerotic plaques *in situ*, leading to increased risk of myocardial infarction and stroke.[16] In addition, under normal homeostatic conditions, arterial wall shear stress is dependent only on the plasma fraction of blood, as RBCs do not come into contact with the endothelium due to the cell-free layer (CFL) created by the Fåhræus–Lindqvist effect.[17,18] Recently, studies have demonstrated that decreasing RBC deformability diminishes or eliminates the CFL, potentially allowing RBCs to come into close proximity and perhaps even transiently have direct contact with the vessel wall.[16] This is particularly pertinent in SCD due to the presence of a small population of irreversibly sickled cells (ISCs) (1-10% of sRBCs), which are permanently rigid and dehydrated. These ISCs have substantially lower deformability from increased cellular viscosity secondary to cellular dehydration and increased membrane rigidity due to oxidative damage.[19,20,21]

Here we present *in vitro* and *in silico* models that demonstrate biophysical alterations of sRBCs may directly induce endothelial dysfunction. Our models show that even small populations of less-deformable RBCs cause significant endothelial dysfunction, with the effects modulated by vessel geometry and the percentage of less-deformable cells. To this end, we leverage a multi-disciplinary approach involving microfluidic systems, cell immunostaining, single-cell RNA sequencing (scRNA-seq), and computational simulations with sRBCs and pharmacologically-dehydrated RBCs (pdRBCs) to address this new biophysical paradigm.

Methods

Endothelialized microfluidic experiments

Blood from healthy donors or individuals with SCD was collected in accordance with IRB protocols and RBCs isolated (Supplemental). To mimic the decreased deformability of sRBCs, healthy RBCs (hRBCs) were pharmacologically-dehydrated with nystatin and high sucrose washes according to established practices to create RBCs with an increased mean corpuscular hemoglobin concentration of 40-42 g/dL.[22] Consent for all patient blood samples was obtained in accordance with Emory University IRB protocol 105125. Consent for all healthy human blood samples was obtained in accordance with Emory University and Georgia Institute of Technology IRB protocol H15258. For all experiments requiring blood at University of Minnesota: Consent for all blood samples was obtained in accordance with Massachusetts General Hospital IRB protocol 2006P000066 and Children's Hospital of Minnesota IRB protocol STUDY00003.

Microfluidic devices (a branching microfluidic device mimicking a small-medium venule in which the smallest microchannels have a 30 μm diameter and a straight 4-channel microfluidic device mimicking a large venule measuring 50 μm high and 100 μm wide) were made from polydimethylsiloxane using standard soft lithography techniques (Supplemental).[23]

A uniform suspension of hRBCs and a binary suspension of 95% hRBCs/5% pdRBCs were perfused through the 50 μm microfluidic device at a volumetric flow rate of 1.25 mL/min for 10 minutes. To determine margination, 5% of RBCs in each suspension (5% hRBCs in the uniform suspension, 5% pdRBCs in the binary suspension) were stained with Octadecyl Rhodamine B Chloride (R18) and a MATLAB-derived program was utilized to visualize R18-stained RBCs (Figure 3B).

After creating the microfluidic devices, the system was ‘‘endothelialized’’ with human umbilical vein ECs (HUVECs) as previously reported (Supplemental). When the device was endothelialized to confluence, hRBCs and sRBCs were isolated, resuspended in media to a 25% hematocrit, and perfused into channels of the microdevice for 4 hours. PdRBCs were created and parallel experiments performed. Hematocrit and plasma free hemoglobin were measured pre- and post-experiment in all conditions with the 50 μm microfluidic device to determine the degree of hemolysis occurring during experimentation. Post-experiment hematocrits ranged from

23.9-24.6% across all conditions. Plasma free hemoglobin differences pre- and post-experiments ranged from 1.5-5% across all conditions except within the 100% pdRBCs, which saw increased hemolysis with a change of 23.6%. After 4 hours, the device was fixed with 4% paraformaldehyde and immunostained with antibodies against VCAM-1 (ABCAM) and E-selectin (Thermo Fisher). The device was then imaged using an inverted optical microscope (10x, Nikon Eclipse TE2000-U), and using ImageJ, mean fluorescence intensity measured (endothelium exposed to hRBCs normalized to 1). For all endothelialized experiments, significance testing was performed using a Mann-Whitney U test (p-value < 0.05).

Computational models of sRBCs

Flowing suspensions of RBCs, modeled as deformable, fluid-filled elastic capsules with discoid radii of 4 μm, were created in straight cylindrical tubes with a 40 μm diameter. RBC membranes incorporated shear elasticity, volume conservation, bending resistance, and area dilatation. The membrane mechanics model and validation against experimental observations were previously modeled by our group.[24]

To mimic a sRBC suspension, binary mixtures of hRBCs with sRBCs were created. In the binary suspensions, the hRBC percentage was 95% or 90% with sRBCs 5% or 10%, respectively. These binary suspension simulations were compared to uniform control suspensions comprised of 100% hRBCs or 100% sRBCs. The overall volume fraction, representing hematocrit, was 20% across suspensions. The suspensions were subjected to unidirectional, pressure-driven flow, and RBC deformability measured (Supplemental).

An immersed boundary method (IBM) was used to measure fluid-structure interactions. Two types of immersed boundaries were considered, including deformable moving cellular membranes and rigid non-moving cylindrical walls. We used "continuous forcing" and "direct forcing" IBM methods for the RBC membranes and tube wall, respectively, with previously described approaches for numerical methology followed.[25,26]

Microfluidic blood rheology deoxygenation experiments

Blood from healthy donors or individuals with SCD was collected in accordance with IRB protocols and RBCs isolated (Supplemental). Plasma was removed following centrifugation at 400xg for 5 minutes and replaced with PBS to a hematocrit of 25%.

Microfluidic systems designed to investigate blood rheology were used as previously described.[27] The microfluidic rheology platform (Figure 4A) allows for perfusion of blood at a fixed pressure, isolated control of reduced oxygen tension to the experimental channel, and simultaneous measurement of RBC velocity profiles using a Kanade–Lucas–Tomasi (KLT) algorithm and MATLAB scripts (Supplemental).

Exchange transfusions of SCD blood samples were prepared *ex vivo* with final percentages of sRBCs totaling 10%, 30%, 70% and 100% of the sample. A 100% hRBCs control was also used. Using the flow profiles generated for each condition, the wall velocity was measured, and the frictional resistance calculated using the known pressure drop across the length of the experimental channel (Supplemental).

ScRNA-seq

ScRNA-seq was performed on ECs collected from our 50 μm microfluidic device after exposure to hRBCs or binary suspensions of 95% hRBCs/5% pdRBCs. Using the previously described protocol, following endothelialization of our microfluidic channels, RBC suspensions of 100% hRBCs or 95% hRBCs/5% pdRBCs were perfused, but following the experiment ECs were trypsinized, resuspended in media, and prepared for scRNA-seq (Supplemental).

ScRNA-seq was performed using a droplet-based ultra-high throughput scRNA-seq system enabling large-scale parallel single-cell gene expression studies. Sequencing was performed using massively-parallel sequencing on the Illumina Novaseq S4 platform, with scRNA-seq analysis performed via established methods

(Supplemental). Differentially expressed genes were calculated using the Wilcoxon rank test with Bonferroni multiple test correction ($p < 0.05$) and enriched pathways were determined using Benjamini-Hochberg adjusted p-values (p-adj. < 0.05).

Results

SRBCs and pdRBCs demonstrate increased endothelial inflammation at bifurcations in endothelialized microfluidic devices mimicking small venules.
ECs were exposed to hRBCs and sRBCs in the 30 μm microfluidic devices mimicking small-medium venules (Figure 1A,B), with parallel experiments completed using hRBCs and pdRBCs. Endothelium exposed to sRBCs and pdRBCs demonstrated increased VCAM-1 and E-selectin expression relative to hRBCs-exposed endothelium (Figure 1C,D), and expression increased as the amount of sRBCs or pdRBCs increased at bifurcations and within the smallest channels, with the highest amount of VCAM-1 and E-selectin expression seen in the 100% sRBC or pdRBCs-exposed endothelium.

SRBCs demonstrate increased margination and local wall shear stress fluctuations in computational simulations.
Computational simulations were created for four RBC suspensions: one uniform suspension containing only hRBCs, one uniform suspension of only sRBCs, and two binary suspensions of hRBCs with small fractions of sRBCs (5% and 10%, respectively) (Figure 2A). As sRBCs are smaller than hRBCs, the number of RBCs in the 100% sRBC suspension is higher than the other suspensions in order to achieve a 20% hematocrit across all suspensions.

The steady-state radial hematocrit profiles for hRBCs, binary sRBC suspensions, and 100% sRBCs illustrate segregation behavior (Figure 2B). SRBCs were found to strongly marginate and travel in higher percentages close to the channel walls in binary suspensions, whereas hRBCs tended to travel in the center of the channel. Interestingly, the 100% sRBCs suspension did not exhibit the same margination behavior, travelling in a distribution similar to that of the hRBCs. This occurs because margination is a phenomenon unique to heterogeneous mixtures, as collisions between hRBCs and sRBCs drives the latter towards the wall.[28,29]

The wall shear stress for the RBC suspensions above was computed to characterize the hydrodynamic effects of RBC distribution on the blood vessel wall. Images of the spatial distribution of additional wall shear stress ($\hat{\tau}_w$) induced by the suspensions are shown (Figure 2C). Blue regions indicate fluctuations of wall shear stress, which increase in the presence of sRBCs and arise at positions corresponding to a near-wall sRBC interaction. These differences are further quantified by the probability density profiles of excess wall shear stress (Figure 2D), as the binary suspensions created large positive fluctuations in wall shear stress compared to the hRBC suspension. This is attributable to sRBC margination. The ratio between these probability densities further highlights large positive fluctuations in wall shear stress that are pronounced in the sRBC binary suspensions. Thus, even when the relative number of sRBCs is small, the relative probability of large stress fluctuations is high.

Aberrant margination of sRBCs and pdRBCs in microfluidic devices mimicking large venules confirm the pathologic local wall shear stresses observed in computational simulations.
Prior to performing additional endothelialized microfluidic experiments, a uniform suspension of hRBCs as well as a binary suspension of 95% hRBCs/5% pdRBCs were perfused through a large venule-mimicking 50 μm microfluidic device (Figure 3A,B). Similar to the results of our computational simulations, pdRBCs traveled in a higher percentage at vessel walls than hRBCs in a uniform suspension (25.8% of stained pdRBCs compared to 4.9% of stained hRBCs traveling within 10 μm of channel walls) (Figure 3C).

Next, ECs were exposed to hRBCs and sRBCs perfused into the same 50 μm microfluidic device, with parallel experiments completed using hRBCs and pdRBCs. (Figure 3D,E). Endothelium VCAM-1 and E-selectin expression increased as the amount of sRBCs increased, similarly to what was observed in our branching microfluidic experiments. As sRBCs were not representative of just ISCs, the binary sickle suspensions likely

did not contain enough of the least-deformable RBCs to lead to increased margination compared to the 100% sRBC suspension. Alternatively, in endothelium exposed to pdRBCs in experiments designed to closely mimic the number of ISCs in SCD blood, binary suspensions with a minority of low-deformability cells showed greater VCAM-1 and E-selectin expression than both the 100% hRBC and pdRBC suspensions, supporting our hypothesis and aligning with computational simulations where there is increased margination and RBC-EC interactions when the less-deformable cells are a minority subpopulation. While transient adhesion cannot be completely ruled out in this system, it is generally not believed to play a significant role in EC inflammation in SCD, and all RBCs were removed from the microfluidics prior to EC immunostaining.

SRBCs exposed to different oxygen concentrations exhibit altered rheological properties with changes in polymerized RBC number in specialized rheological microfluidics.

RBC velocity profiles show a decrease in average velocity due to decreases in both wall velocity (V_{wall}) and maximum velocity (V_{max}) in sRBC suspensions exposed to 21% and 0% oxygen, respectively (Figure 4B). To study the direct effect of polymerized sRBCs on bulk rheology, an exchange transfusion technique was utilized to compare rheological properties at 0% and 21% oxygen. Exchange transfusions of SCD blood samples were prepared to final sRBCs percentages totaling 10%, 30%, 70% and 100%. A 100% hRBCs control showed no difference in frictional resistance at 0% oxygen (Supplemental Figure 2). Using the flow profiles generated for each condition, V_{wall} was measured, and the frictional resistance was calculated using the known pressure drop across the length of the experimental channel (Supplemental). Rheological analysis for each transfusion ratio showed an increase in frictional resistance at 0% oxygen compared to 21% oxygen indicating that the presence of sRBCs perturbs the rheology near the channel walls (Figure 4C-F). Additionally, the magnitude of the frictional resistance at 0% oxygen increased as the number of sRBCs increased as indicated by the high transfusion ratio samples. These results couple nicely with our computational and endothelialized microfluidic data to elicit the alterations in blood flow, RBC-EC interactions, and subsequent endothelial dysfunction.

ScRNA-seq reveals changes in the transcriptome of ECs exposed to heterogeneous RBC suspensions with a subpopulation of pdRBCs.

To determine the effect of less-deformable RBCs on gene expression, scRNA-seq data was generated from ECs after exposure to hRBCs or binary suspensions of hRBCs with a small subpopulation of pdRBCs. Clustering of the hRBCs and pdRBC-exposed ECs based on transcriptomic profiles resulted in eight distinct clusters visualized by Uniform Manifold Approximation and Projection (UMAP) (Figure 5A). ECs exposed to binary suspensions showed reduced proportions of clusters C and D and increased proportions of clusters E and F compared to hRBC-exposed ECs (Figure 5B). Top markers associated with each cluster (Figure 5C) showed hRBC-enriched clusters display upregulation of genes associated with cellular proliferation and migration. In contrast, pdRBC-exposed ECs demonstrate an upregulation of stress response genes and key regulatory factors of endothelial activation (Supplemental). Pathway enrichment analysis further supported these findings (Figure 5D), as hRBC-associated clusters exhibit significant enrichment (p-adj. < 0.05) of cellular motility and cell cycle pathways. Conversely, pdRBC-associated clusters showed significant upregulation of oxidative stress pathways, including iron uptake and ROS/RNS production, as well as increased cellular activation via kinase and transcription factor activity. Lastly, to investigate which genes were driving the transcriptomic differences between the hRBC and pdRBC-exposed ECs, a volcano plot was generated (Figure 5E). Several notable genes were observed to be significantly upregulated ($p < 0.00001$) following pdRBC exposure, including known markers of endothelial activation following injury and a key regulator of endothelial remodeling in response to disturbed flow.[30] Interestingly, markers of ferroptosis were also upregulated, suggesting ferroptosis may play a role in endothelial dysfunction (Supplemental).[31] These results reinforce our earlier findings that RBC deformability influences blood flow, inducing shear stress and subsequent endothelial activation via the upregulation of oxidative stress pathways and key factors involved in endothelial injury response.

Discussion

Overall, this work describes and uncovers a "missing biophysical link" in our understanding of SCD pathophysiology that explains how the decreased deformability of the sRBCs, in and of itself, can cause diffuse vascular dysfunction throughout the entire circulation via mechanobiological pathways that are completely independent of cell adhesion, hemolysis, and vaso-occlusion. Moreover, our data provides insight into how this newfound process contributes to alterations in flow within larger vessels down to the microvasculature. To the best of our knowledge, no previous studies have directly correlated (1) these aforementioned processes, (2) that less-deformable RBCs can cause aberrant compressive forces in the microvasculature, (3) increased RBC margination and subsequent altered wall shear stress fluctuations in larger vessels, and (4) that all of these cause endothelial dysfunction in SCD.

Here, we leveraged a multi-disciplinary approach of microfluidics, computational simulations, and scRNA-seq with sRBCs as well as pdRBCs to explore this new pathophysiologic paradigm that purely biophysical alterations of RBCs in SCD are sufficient to cause endothelial dysfunction (Figure 6). First, we leveraged small venule-mimicking, microfluidic devices to explore if less-deformable RBCs have increased interactions with the endothelium at bifurcations leading to increased endothelial dysfunction as measured by surface expression of VCAM-1 and E-selectin.

Moreover, our computational simulations demonstrated that the less-deformable sRBC subpopulations exhibit increased margination towards channel walls, altering the CFL and causing increased fluctuations in localized shear stress not observed in the homogeneous hRBC suspension. Additional microfluidic experiments confirmed these results using a large venule-mimicking microfluidic device. Importantly, binary suspensions with a subpopulation of pdRBCs yielded the highest VCAM-1 and E-selectin expression.

Our work was designed to isolate physical interactions by eliminating the role of biochemical ones, and a CFL remained even in the absence of aggregation both experimentally and within our simulations. While RBC aggregation, a complex process involving biochemical interactions mediated by plasma proteins such as fibrinogen, will influence the CFL, we demonstrate that the CFL occurs even in its absence, as the CFL and margination phenomena can arise purely from mechanical interactions between cells. The biophysical effects of RBC aggregates on endothelial dysfunction in SCD are currently being studied by our group, but beyond the scope of this paper.

Given the limited methods to measure microcirculation blood rheological parameters, we also developed a method coupling microfluidics and object-tracking technologies with mathematical modeling to separate RBC flow profiles into bulk and wall components,[32] allowing for the evaluation of bulk viscosity and wall friction contributions to the overall resistance in SCD blood under a range of oxygen tensions. To explore the effect of deoxygenation, we quantified local rheological changes in sRBC suspensions such as frictional resistance, the resistance to RBC flow near channel walls. Quantifying frictional resistance is important as shear stress is highest near vessel walls, particularly in small vessels with a high surface area: volume ratio. While the CFL lowers frictional resistance, margination of cells disrupting this layer will increase frictional resistance, resulting in an increase in overall viscosity. Additionally, artificial transfusions of sRBCs with hRBCs allowed us to test the direct effect of polymerized sRBCs on local rheology by subjecting the sample to 0% oxygen. An increase in frictional resistance at 0% oxygen compared to 21% oxygen was observed even at modest transfusion ratios showing the presence of small amounts of less-deformable cells disrupts flow near the wall. Furthermore, increasing the sRBC: hRBC ratio resulted in increasing frictional resistance in the deoxygenated case. Our results offer biophysical insight into the pathological role less-deformable cells due to HbS polymerization might have on endothelial dysfunction under physiological conditions and are consistent with the dose-dependent effect these cells had on endothelial activation in prior experiments.

Finally, scRNA-seq was performed on ECs exposed to hRBCs and a binary suspension with hRBCs and pdRBCs to determine if less-deformable RBCs can induce differential gene expression. Differentially expressed genes involved in ROS, RNS, TGFB, and interleukin signaling were observed in ECs exposed to pdRBCs in

comparison to hRBCs. Another interesting finding was the increase in differential gene expression of Krüppel-like factors 4 (*Klf4*) and 6 (*Klf6*) in pdRBC-exposed ECs, as the KLF family of transcription factors have both developmental and pathologic implications within the vasculature.[33] *Klf4* has been shown to be a regulator of endothelial activation in response to proinflammatory stimuli and shear stress,[34] while *Klf6* plays a role in vascular development, remodeling, and injury response.[35] Additionally, we saw upregulation in *MARCKSL1* in pdRBC-exposed ECs, which produces an actin-binding protein responsible for modulating mechanical properties of the EC cortex to regulate cell shape and vessel structure during angiogenesis. Increased expression leads to an increase in both EC size and microvessel diameter,[36] potentially explaining a mechanism of pathologic alterations of the cerebrovasculature in SCD.

Our scRNA-seq results confirm that transcription-level alterations occur in ECs when exposed to biophysically altered RBCs. While previous studies have shown that these aforementioned pathways are involved in mechanotransduction in the context of how alterations in flow affects EC gene expression,[37,38] ours is the first to demonstrate that perfusion of biophysically-altered RBCs also affects these pathways in ECs. These transcriptional changes explore early EC responses to biophysical RBC alterations. Further longitudinal experiments and subsequent data have the potential to yield even more meaningful results, particularly in determining which EC responses are mechanotransductive processes in direct response to aberrant physical forces.

Overall, this work helps elucidate the ubiquity of vascular dysfunction in SCD and has the potential to lead to a new paradigm of biophysical therapeutic strategies directed towards mitigating aberrant RBC margination in SCD (e.g., erythrocytapheresis to intravenously remove the stiffest RBC populations). In addition to evaluating this paradigm across different flow regimes, such as in the disturbed flow of the intricate cerebral vasculature, ongoing efforts involve the development of a mouse model to study this new paradigm of how the biophysical properties of sRBCs lead to pathologic fluidic and mechanical forces that, in turn, drive SCD vasculopathy *in vivo*.

Acknowledgements

This work was supported by an American Society of Hematology (ASH) Research Training Award for Fellows (RTAF), National Institutes of Health, Institute of Heart, Lung, and Blood (NIH NHLBI) grant T32HL139443, Pediatric Loan Repayment Program (LRP) Award L40HL149069, and Atlanta Pediatric Scholars Program sponsored by the NICHD Child Health Research Career Development Award Program grant K12HD072245 (C.C.), National Institutes of Health, Institute of Heart, Lung, and Blood (NIH NHLBI) grants R01HL140589 and R35HL145000 (W.A.L.), and National Science Foundation grant CBET-2042221 (X.C. and M.D.G.).

Authorship Contributions

C.C. and W.A.L. designed the study; X.C. and M.D.G. designed and created computational simulations; H.M.S. and D.K.W. designed and performed rheological microfluidic experiments; B.E.T., M.E.M., and M.B. performed scRNA-seq and its associated statistical analysis; C.C. performed microfluidic experiments; X.Z., M.E.F., R.G.M., Y.S. and D.R.M. designed and performed preliminary experiments; W.L. and C.H.J. developed and helped perform nystatin treatment of RBCs; C.C., X.C., H.M.S., M.E.M., B.E.T. performed data analysis; C.C. wrote the article, all authors reviewed and edited the article; M.B., M.D.G. and W.A.L. oversaw the project.

Conflict of Interest Disclosures

The authors declare no competing interests.

References

[1] Pauling L, Itano HA, et al. Sickle cell anemia a molecular disease. Science. 1949;110(2865):543-8. Epub 1949/11/25. doi: 10.1126/science.110.2865.543.
[2] Rabai M, Detterich JA, Wenby RB, et al. Deformability analysis of sickle blood using ektacytometry. Biorheology. 2014;51(0):159-170. https://doi.org/10.3233%2FBIR-140660
[3] Tripette J, Alexy T, Hardy-Dessources M-D, et al. Red blood cell aggregation, aggregate strength and oxygen transport potential of blood are abnormal in both homozygous sickle cell anemia and sickle-hemoglobin C disease. Haematologica. 2009;94(8):1060-1065. https://doi.org/10.3324/haematol.2008.005371
[4] Alapan Y, Matsuyama Y, Little JA, Gurkan UA. Dynamic deformability of sickle red blood cells in microphysiological flow. Technology. 2016;4(2):71-79. doi: 10.1142/S2339547816400045.
[5] Bunn HF, Nathan DG, Dover GJ, Hebbel RP, Platt OS, Rosse WF, Ware RE. Pulmonary hypertension and nitric oxide depletion in sickle cell disease. Blood. 2010;116(5):687-92. Epub 2010/04/17. doi:10.1182/blood-2010-02-268193blood-2010-02-268193
[6] Kato GJ, Hebbel RP, Steinberg MH, Gladwin MT. Vasculopathy in sickle cell disease: Biology, pathophysiology, genetics, translational medicine, and new research directions. Am J Hematol. 2009; 84(9):618-25. Epub 2009/07/18. doi: 10.1002/ajh.21475.
[7] Morris CR. Mechanisms of vasculopathy in sickle cell disease and thalassemia. Hematology Am Soc Hematol Educ Program. 2008:177-85. Epub 2008/12/17. doi: 10.1182/asheducation-2008.1.177 2008/1/177
[8] Aessopos A, Farmakis D, Tsironi M, Diamanti-Kandarakis E, Matzourani M, Fragodimiri C, Hatziliami A, Karagiorga M. Endothelial function and arterial stiffness in sickle-thalassemia patients. Atherosclerosis. 2007;191(2):427-32. doi: 10.1016/j.atherosclerosis.2006.04.015.
[9] Kato GJ, Gladwin MT. Evolution of novel small-molecule therapeutics targeting sickle cell vasculopathy. Jama. 2008;300(22):2638-46. doi: 10.1001/jama.2008.598
[10] Yuditskaya S, Tumblin A, Hoehn GT, Wang G, Drake SK, Xu X, Ying S, Chi AH, Remaley AT, Shen RF, Munson PJ, Suffredini AF, Kato GJ. Proteomic identification of altered apolipoprotein patterns in pulmonary hypertension and vasculopathy of sickle cell disease. Blood. 2009;113(5):1122-8. doi: 10.1182/blood-2008-03-142604.
[11] Abe J, Berk BC. Novel mechanisms of endothelial mechanotransduction. Arterioscler Thromb Vasc Biol. 2014;34(11):2378-86. doi: 10.1161/ATVBAHA.114.303428
[12] Chien S. Mechanotransduction and endothelial cell homeostasis: the wisdom of the cell. Am J Physiol Heart Circ Physiol. 2007;292(3):H1209-24. doi: 10.1152/ajpheart.01047.2006.
[13] Harrison DG, Widder J, Grumbach I, Chen W, Weber M, Searles C. Endothelial mechanotransduction, nitric oxide and vascular inflammation. J Intern Med. 2006;259(4):351-63. doi: 10.1111/j.1365-2796.2006.01621.x.
[14] Chatterjee, S, Fisher, AB. Mechanotransduction in the Endothelium: Role of Membrane Proteins and Reactive Oxygen Species in Sensing, Transduction, and Transmission of the Signal with Altered Blood Flow. Antioxid Redox Signal. 2014; 20(6): 899-913. Doi: 10.1089/ars.2013.5624
[15] Schulz, E, Gori, T, Munzel, T. Oxidative stress and endothelial dysfunction in hypertension. Hypertens Res. 2011; 34: 665-673.
[16] Abe, J, and Berk, BC. Novel mechanisms of endothelial mechanotransduction. Arterioscler. Thromb. Vasc. Biol. 2014; 34, 2378–2386. Doi: 10.1161/ATVBAHA.114.303428.
[17] Fahraeus R, Lindqvist T. The viscosity of the blood in narrow capillary tubes. American Journal of Physiology. 1931;96:562-8. doi: 10.1152/ajplegacy.1931.96.3.562
[18] Goldsmith HL, Skalak R. Hemodynamics. Annual Review Of Fluid Mechanics. 1975;7:213-47. Doi: 10.1146/annurev.fl.07.010175.001241
[19] Asakura T, Mattiello JA, Obata K, Asakura K, Reilly MP, Tomassini N, Schwartz E, Ohene-Frempong K. Partially oxygenated sickled cells: sickle-shaped red cells found in circulating blood of patients with sickle cell disease. Proc Natl Acad Sci U S A. 1994;91(26):12589-93. doi: 10.1073/pnas.91.26.12589

[20] Clark MR, Mohandas N, Shohet SB. Deformability of oxygenated irreversibly sickled cells. J Clin Invest.1980;65(1):189-96. Epub 1980/01/01. doi: 10.1172/JCI109650.
[21] Nash GB, Johnson CS, Meiselman HJ. Rheologic impairment of sickle RBCs induced by repetitive cycles of deoxygenation-reoxygenation. Blood. 1988;72(2):539-45. Doi: 10.1182/blood.V72.2.539.539
[22] Joiner, CH, Lauf, PK. Modulation of Ouabain Binding and Potassium Pump Fluxes by Cellular Sodium and Potassium in Human and Sheep Erythrocytes. J Physiol. 1978; 283: 177-196. Doi: 10.1113/jphysiol.1978.sp012495.
[23] Hoelzle, DJ, Varghese, BA, Chan, CK, and Rowat, AC. A microfluidic technique to probe cell deformability. J. Vis. Exp. 91, e51474. Doi:10.3791/51474.
[24] Sinha, K, and Graham, MD. Dynamics of a single red blood cell in simple shear flow. Phys Rev E. 2015; 92, 042710. https://doi.org/10.1103/PhysRevE.92.042710.
[25] Balogh, P, Bagchi, P. A computational approach to modeling cellular scale blood flow in complex geometry. J Comput Phys. 2017; 334, 280–307. https://doi.org/10.1016/j.jcp.2017.01.007.
[26] Mittal, R, Dong, H, Bozkurttas, M, Najjar, FM, Vargas, A, and von Loebbecke, A. (2008). A versatile sharp interface immersed boundary method for incompressible flows with complex boundaries. J Comput Phys. 2008; 227, 4825–4852. https://doi.org/10.1016/j.jcp.2008.01.028.
[27] Valdez, JM, Datta, YH, Higgins, JM, Wood, DK. A microfluidic platform for simultaneous quantification of oxygen-dependent viscosity and shear thinning in sickle cell blood. APL Bioeng, 2019; 3(4), 046102. Doi:10.1063/1.5118212, https://doi.org/10.1063/1.5118212
[28] Kumar, A, Graham, MD. Mechanism of margination in confined flows of blood and other multicomponent suspensions. Phys Rev Lett. 2012; 109(10), 108102. Doi:10.1103/PhysRevLett.109.108102.
[29] Cheng, X, Caruso, C, Lam, WA, Graham, MD. Marginated aberrant red blood cells induce pathologic vascular stress fluctuations in a computational model of hematologic disorders. bioRxiv 2023.05.16.541016. Doi: 10.1101/2023.05.16.541016.
[30] Kondrychyn, I, Kelly, DJ, Carretero, NT, Nomori, A, Kato, K, Chong, J, Nakajima, H, Okuda, S, Mochizuki, N, Phng, LK. Marcksl1 modulates endothelial cell mechanoresponse to haemodynamic forces to control blood vessel shape and size. Nat Commun. 2020; 11: 5476 Doi: 10.1038/s41467-020-19308-5
[31] Zhang, H, Zhou, S, Sun, M, Hua, M, Liu, Z, Mu, G, Wang, Z, Xiang, Q, Cui, Y. Ferroptosis of Endothelial Cells in Vascular Diseases. Nutrients. 2022; 14(21): 4506. Doi: 10.3390/nu14214506
[32] Szafraniec, HM, Valdez, JM, Iffrig, E, Lam, WA, Higgins, JM, Pearce, P, Wood, DK. Feature tracking microfluidic analysis reveals differential roles of viscosity and friction in sickle cell blood. Lab Chip. 2022; 22, 1565-1575. Doi: 10.1039/d1lc01133b.
[33] Suzuki, T, Aizawa, K, Matsumura, T, Nagai, R. Vascular Implications of the Kruppel-Like Family of Transcription Factors. Arterioscl Throm Vas. 2005; 25(6): 1135-1141. Doi: 10.1161/01.ATV.0000165656.65359.23
[34] Hamik, A, Lin, Z, Kumar, A, Balcells, M, Sinha, S, Katz, J, Feinberg, M, Gerzsten, RE, Edelman, ER, Jain, MK. Kruppel-like factor 4 regulates endothelial inflammation. J Biol Chem. 2007; 282: 13769–13779. Doi: 10.1074/jbc.M700078200
[35] Atkins, GB, Jain, MK. Role of Kruppel-Like Transcription Factors in Endothelial Biology. Circ Res. 2007; 100(12): 1686-1695. Doi: 10.1161/01.RES.0000267856.00713.0a
[36] Kondrychyn, I, Kelly, DJ, Carretero, NT, Nomori, A, Kato, K, Chong, J, Nakajima, H, Okuda, S, Mochizuki, N, Phng, LK. Marcksl1 modulates endothelial cell mechanoresponse to haemodynamic forces to control blood vessel shape and size. Nat Commun. 2020; 11: 5476 Doi: 10.1038/s41467-020-19308-5
[37] Jeng-Jiann, C, Yi-Shuan, L, Chien, S. Focal adhesion kinase phosphorylation in flow-activation of endothelial NF-jB. Focus on 'focal adhesion kinase modulates activation of NF-jB by flow in endothelial cells. Am J Physiol Cell Physiol. 2009; 297(4): C800–801. Doi: 10.1152/ajpcell.00364.2009
[38] He, M, Martin, M, Marin, T, Chen, Z, Gongol, B. Endothelial mechanobiology. APL Bioeng. 2020; 4(1): 010904. Doi: 10.1063/1.5129563

Figure Legends

Figure 1: Endothelial cells exposed to pharmacologically-dehydrated and sickled RBCs demonstrate increased endothelial inflammation within the smallest channels and at bifurcations in microfluidic devices mimicking small venules.
(A) Macroscopic view of a microfluidic device designed to mimic a small-medium venule, where the smallest channels are ~30 μm in diameter. (B) Brightfield microscopy image at 10x magnification of the initial branchpoint of our small-medium venule-mimicking microfluidic device endothelialized to confluence with human umbilical vein endothelial cells. (C) Endothelial VCAM-1 (green) and E-selectin (red) expression in the first branchpoint of the microfluidic device after 4-hour perfusion of healthy control RBCs versus RBC suspensions containing varying amounts (5%, 10%, and 100%) of sickle RBCs (left) and nystatin-treated, less-deformable RBCs (right). All RBC suspensions were diluted in media to a hematocrit of 25% and perfused at a constant venular shear rate. (D) Graphical representation of mean normalized fluorescent intensity for VCAM-1 and E-selectin, both markers of inflammation, in endothelial cells exposed to healthy RBCs (red) and RBC suspensions with varying amounts of sickle RBCs (left graph) and nystatin-treated, less-deformable RBCs (right graph) at the initial branchpoint shown. A total of 5 separate experiments were analyzed. VCAM-1 and E-selectin expression increased as the number of sickled RBCs increased. In the experiments utilizing nystatin-treated RBCs, VCAM-1 and E-selectin had a statistically significant increase in expression as the number of less-deformable cells increased (VCAM-1 2.29 ± 0.46 SEM ($p<0.05$), E-selectin 1.7 ± 0.16 SEM ($p<0.05$) normalized fluorescent intensity in endothelial cells exposed to 100% nystatin-treated RBCs), indicating that increased RBC-endothelial cell interactions occur at vessel branchpoints in the presence of less-deformable RBCs, which also exert increased compressive mechanical forces against the endothelium in the smallest vessels. (Statistical analyses: $*p \leq 0.05$ using a Mann-Whitney U test. Error bars represent SEM).

Figure 2: Sickle RBC subpopulations demonstrate increased margination and induce local wall shear stress fluctuations in computational simulations.
(A) Angled views of snapshots taken from computational simulations of RBC suspensions comprised entirely of healthy RBCs (left), binary suspensions with a majority of healthy RBCs and a minority population of sickle RBCs comprising 5% (second) and 10% (third) of the overall suspension, and a suspension comprised entirely of sickle RBCs (right). Each simulation was conducted with a hematocrit of 20%. As sickle RBCs have a smaller size than healthy RBCs, there is a larger number of total RBCs in the 100% sickle RBC suspension. Binary suspensions were designed to mimic ISCs in individuals with SCD. A cell-free layer can be observed in homogeneous suspensions comprised of 100% healthy RBCs or 100% sickle RBCs, while in binary suspensions, marginated sickle cells are concentrated within the cell-free layer close to channel walls. (B) Steady state radial hematocrit profiles (Ht) for healthy RBCs (red) and sickle RBCs (blue) in RBC suspensions containing 0%, 5%, 10%, and 100% sickle RBCs, respectively. The x-axis depicts distance from the center of the channel scaled with the radius of a healthy RBC, with 0 being the center of the channel and 5 representing the channel walls. In all cases the hematocrit of the healthy RBCs, as well as sickle RBCs in the 100% sickle RBC suspension, drops precipitously close to the wall, corresponding to the cell-free layer. In binary suspensions, sickle RBCs tend to marginate and travel in higher percentages within the cell-free layer close to channel walls, whereas healthy RBCs concentrate around the center of the channel. Sickle RBCs in the 100% sickle RBC suspension did not exhibit the same margination, maintaining the cell-free layer; this can be attributed to the presence of deformable, healthy RBCs in the binary suspensions, which drive the sickle RBCs towards the walls. (C) Snapshot of the spatial distribution of additional wall shear stress ($\hat{\tau}_w$) induced by healthy RBCs (left), binary sickle RBC suspensions comprised of 5% (second) and 10% (third) sickle RBCs,

and 100% sickle RBCs (right), respectively. Blue regions indicate large fluctuations and are more numerous in the presence of sickle RBCs. (D) Probability density profile of excess wall shear stress induced by varying fractions of sickle RBCs (left). The binary suspensions created large fluctuations in wall shear stress in comparison to the healthy RBC suspension. The ratio between probability densities (right) shows large positive fluctuations in wall shear stress in binary suspensions of 5 and 10% sickle RBCs.

Figure 3: Heterogeneous suspensions containing pharmacologically-dehydrated and sickled RBCs exhibit margination towards vessel walls leading to increased endothelial dysfunction in large venule-mimicking microfluidic systems.

(A) Macroscopic view of a 50 x 100 μm straight-channel microfluidic device designed to mimic a large venule. (B) Cartoon depiction of our microfluidic experimental set-up and corresponding video snapshot of a superposition of brightfield and fluorescence microscopy images of an RBC suspension comprised of 5% pharmacologically-dehydrated, less-deformable RBCs (stained with R18) and 95% healthy RBCs flowing through a straight microfluidic channel with a diameter of 100 μm at a constant flow rate. R18-stained RBCs travelling close to the channel wall as well as more centrally in the channel are circled by a dashed yellow line and solid line, respectively. (C) Graphical representation of the experiment shown in (B), comparing an RBC suspension comprised of 100% healthy RBCs (5% RBCs stained) with an RBC suspension with a majority healthy (95%) RBC population with a minority (5%) less-deformable and stained RBCs. Software analysis tracking of the stained RBCs was performed, and showed that in comparison to healthy RBCs, less-deformable RBCs were more likely to marginate and travel in close proximity to vessel walls. (D) Endothelial VCAM-1 (green) and E-selectin (red) expression after 4-hour perfusion of healthy control RBCs versus RBC suspensions containing varying amounts (5%, 10%, and 100%) of sickle RBCs. All RBC suspensions were diluted in media to a hematocrit of 25% and perfused at a constant venular shear rate. Graphical representation of mean normalized fluorescent intensity for VCAM-1 (left) and E-selectin (right), both markers of inflammation, in endothelial cells exposed to healthy RBCs (red) and RBC suspensions with varying amounts of sickle RBCs in the straight-channel microfluidic is also shown. A total of 5 separate experiments were analyzed. VCAM-1 and E-selectin expression increased as the amount of sickle RBCs increased (VCAM-1 1.35 ± 0.12 SEM ($p<0.05$), E-selectin 1.29 ± 0.10 SEM ($p<0.05$) normalized fluorescent intensity in the 100% sickle RBC-exposed endothelial cells). As sickle RBCs do not represent only ISCs (i.e., the least deformable RBCs), the 5 and 10% sickle suspensions likely did not contain enough of the least deformable RBCs to lead to increased margination in comparison to the 100% sickle RBC suspension. (E) Endothelial VCAM-1 and E-selectin expression after 4-hour perfusion of healthy control RBCs versus RBC suspensions containing varying amounts (5%, 10%, and 100%) of nystatin-treated RBCs, with mean normalized fluorescent intensity for VCAM-1 (left) and E-selectin (right) in endothelial cells exposed to healthy RBCs (red) and RBC suspensions with varying amounts of nystatin-treated RBCs in the straight-channel microfluidic. A total of 5 separate experiments were analyzed. VCAM-1 and E-selectin expression in heterogeneous suspensions with a minority of less-deformable cells at 5 or 10% of the total suspension showed greater expression than the 100% low-deformability suspension (VCAM-1 1.7 ± 0.17 SEM ($p<0.05$), E-selectin 2.91 ± 1.56 SEM ($p< 0.05$) normalized fluorescent intensity highest in 10% nystatin-treated RBC-exposed endothelial cells), supporting our hypothesis that when the less-deformable cells are a minority subpopulation, there is increased margination and RBC-endothelial cell interactions and subsequent dysfunction. (Statistical analyses: $*p \leq 0.05$ using a Mann-Whitney U test. Error bars represent SEM).

Figure 4: Microfluidic analysis of SCD red blood cell properties indicate changes in rheological properties in blood flow as the quantity of polymerized red blood cells changes for both native and transfused blood.

(A) The microfluidic rheology platform consists of a multilayer microfluidic device with a bifurcating blood channel designed to mimic the cross-sectional area of a small arteriole or venule as shown. The device allows

for perfusion of blood at a fixed pressure, isolated control of reduced oxygen tension to the experimental channel, and simultaneous measurement of RBC velocity profiles using the KLT algorithm and custom Matlab scripts. All blood samples were prepared to a hematocrit of 25% in PBS. (B) RBC velocity profiles for one SCD patient blood sample subjected to 21% oxygen and 0% oxygen showed a decrease in average velocity while demonstrating decreases in both the wall velocity (V_{wall}) and the max velocity (V_{max}). (C-F) The direct effect of polymerized sickle RBCs on bulk rheology is determined using an exchange transfusion technique and measuring rheological properties at 0% oxygen and comparing to the 21% oxygen condition immediately prior to cycling oxygen off. Exchange transfusions of SCD blood samples are prepared *ex vivo* at ratios of 10%, 30%, 70% and 100% SCD blood. Rheological analysis shows an increase in the frictional resistance for each condition indicating that the presence of sickled RBCs impedes flow near the channel walls. (Statistical analyses: *$p \leq 0.05$, **$p \leq 0.01$, ***$p \leq 0.001$, and ****$p \leq 0.0001$ using Welch's t test).

Figure 5: Single cell RNA sequencing (scRNA-seq) reveals differential endothelial cell gene expression in endothelialized microfluidic devices exposed to a heterogeneous RBC suspension with a subpopulation of less-deformable RBCs in comparison to a homogeneous RBC suspension of healthy RBCs.
Using the same 50 x 100 μm microfluidic device endothelialized to confluence with human umbilical vein endothelial cells and RBC preparations as previously described (5% nystatin-treated with 95% healthy RBCs compared to 100% healthy RBCs), RBC suspensions were again perfused for 4 hours, but following the experiment endothelial cells were collected and prepared for scRNA-seq. (A) Uniform Manifold Approximation and Projection (UMAP) embedding of scRNA-seq samples consisting of high-quality endothelial cells portioned into eight clusters with unique transcriptomic profiles. (B) Distribution of endothelial cell clusters following healthy versus nystatin-treated, low deformability RBC exposure. Following exposure to nystatin-treated RBCs, a reduction in clusters C and D with a concomitant increase in clusters E and F was observed. (C) A heatmap displaying the top markers expressed within each cluster. Columns represent individual cells, grouped by clusters, and rows display individual genes with the highest differential expression within each subcluster. Color bar shows gene expression levels with red being high and blue low gene expression. Healthy RBC enriched clusters C and D display an upregulation of genes associated with cellular proliferation and migration, including *FP671120* (miR-3648), *COL4A1* (collagen type IV), *MKI67* (Ki-67), and *CKS1B* (CDC28 protein kinase regulatory subunit 1B). In contrast, clusters E and F, associated with nystatin-treated RBC exposure, demonstrate an upregulation of stress response genes, such as *SRXN1* (sulfiredoxin 1) and *ERG1* (early growth response protein 1), as well as several key regulatory factors involved in endothelial activation, including *ANKRD1* (cardiac ankyrin repeat protein), *KLF4* (Krüppel-like factor 4), *FOS*, and *JUN*. (D) Pathways enriched in each endothelial cell cluster. Clusters C and D, which were reduced in endothelial cells exposed to nystatin-treated RBCs, are notably enriched in cellular proliferation and motility pathways, namely those involving RHO GTPase, laminin, integrin, and ECM proteoglycans, in addition to cell cycle pathways. Clusters E and F, enriched following nystatin-treated RBC exposure, exhibited significant enrichment of cellular response and oxidative stress pathways, including iron uptake, NFE2L2 signaling, and ROS and RNS production, as well as enriched cellular response and regulatory activity via kinase and transcription factor activation pathways. (E) A volcano plot illustrating differential gene expression in endothelial cells exposed to nystatin-treated, low deformability RBCs versus healthy RBCs, wherein genes upregulated following nystatin-treated RBC exposure show a positive fold-change, while upregulated following healthy RBC exposure show a negative fold-change ($p < 0.00001$). Several notable genes were observed to be significantly upregulated following nystatin-treated RBC exposure such as known markers of endothelial activation following injury, including *THBS1*, *MMP1*, *CXCL8*, *EEF1A1*, *KLF6*, and *FN1*. *MARCKSL1*, a key regulator of endothelial remodeling in response to disturbed flows, was also found to be upregulated. Markers of ferroptosis, *GPX4*, *ATF3*, *PTGS2*, and *FTH1* were also upregulated.

Figure 6: Biophysical alterations of less-deformable and sickled RBCs directly induce endothelial inflammation via margination and increased RBC-endothelial interactions.
Cartoon representation of our new paradigm of SCD vasculopathy, showing that when RBC suspensions are not uniform, such as in SCD, a subpopulation of the smallest and least deformable sickle RBCs will tend to enter the cell free layer and marginate closer to vessel walls. These marginating RBCs not only come into direct contact (i.e. RBC-endothelial cell collisions) with the endothelium but also create altered local wall shear stress simply from coming into close proximity to the vessel wall, inducing endothelial inflammation via mechanobiological mechanisms. Furthermore, as these less-deformable and sickle RBCs flow into smaller areas of more complex geometries, such as at bifurcations, additional brief, collision-like events will occur secondary to their altered flow patterns, causing further exposure to increased mechanical forces. Finally, as sickle RBCs squeeze into the capillaries, endothelial cells are exposed to pathologically increased compressive mechanical forces, which again induce a pro-inflammatory phenotype via mechanotransduction.

Figure 1

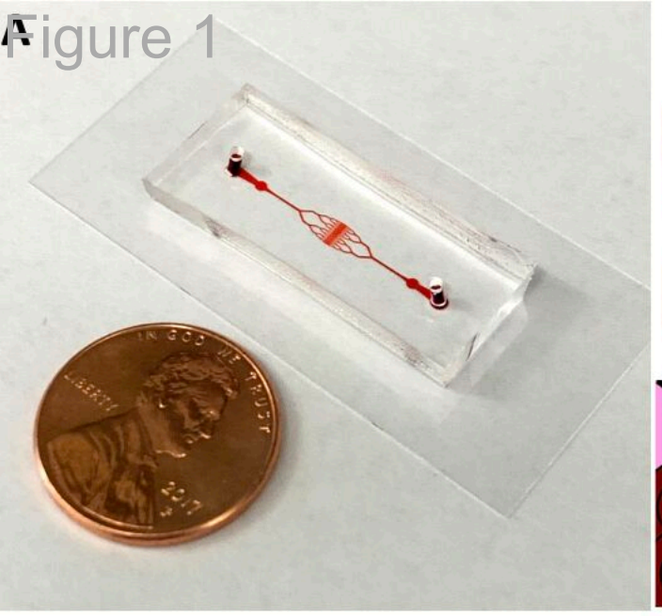

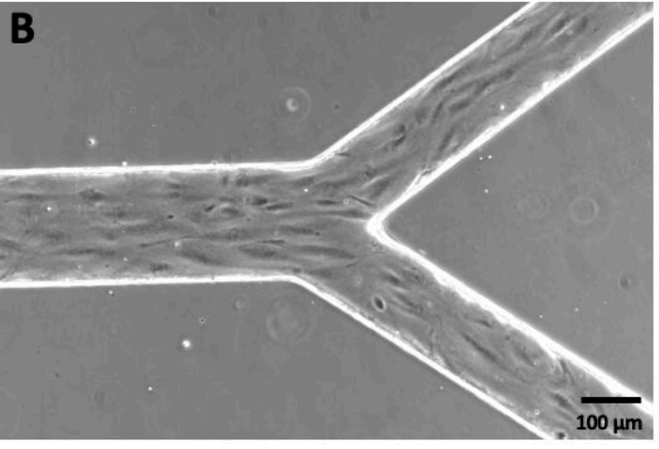

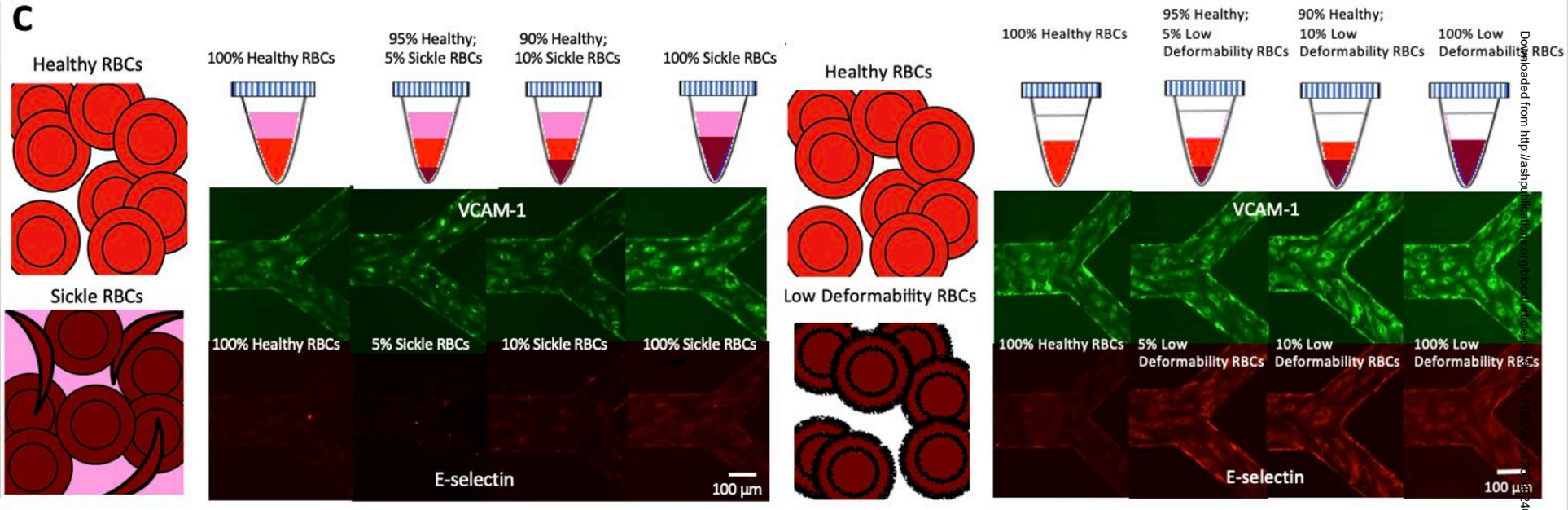

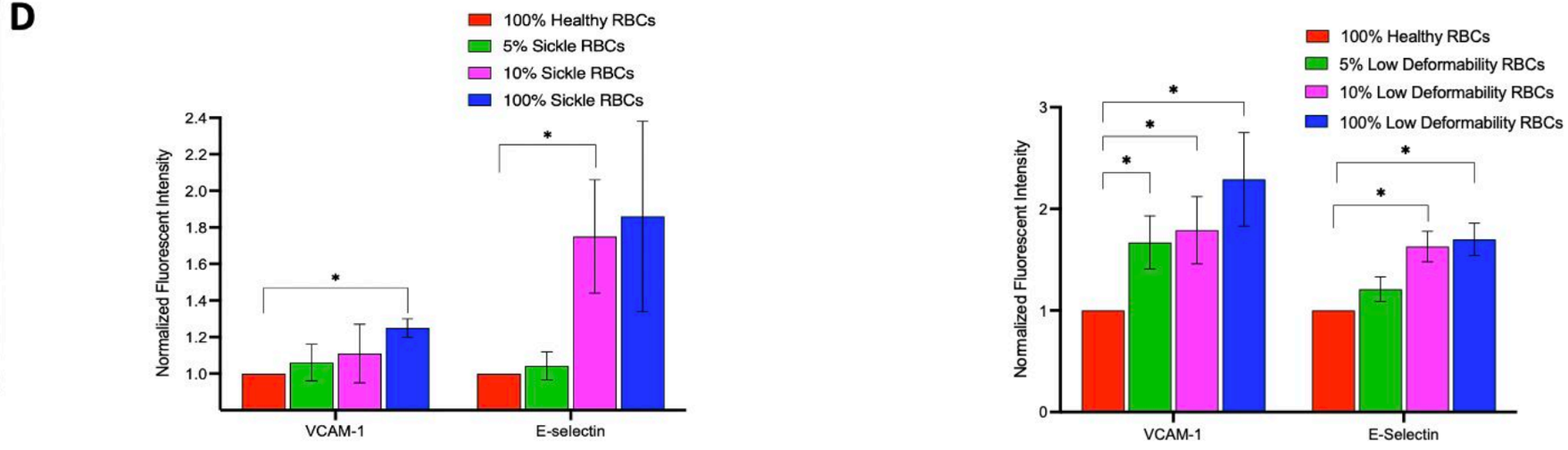

Figure 2

A

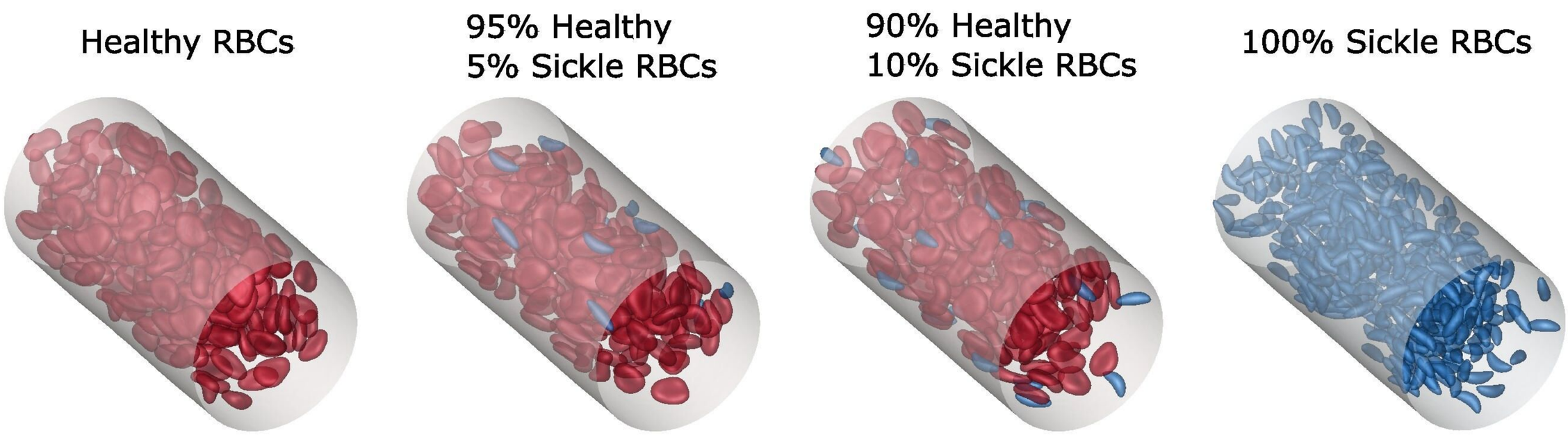

B

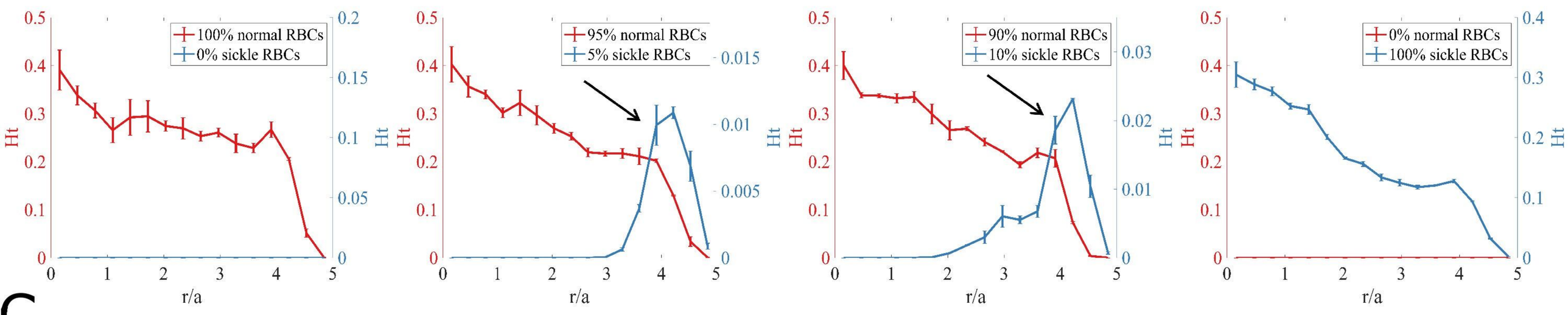

C

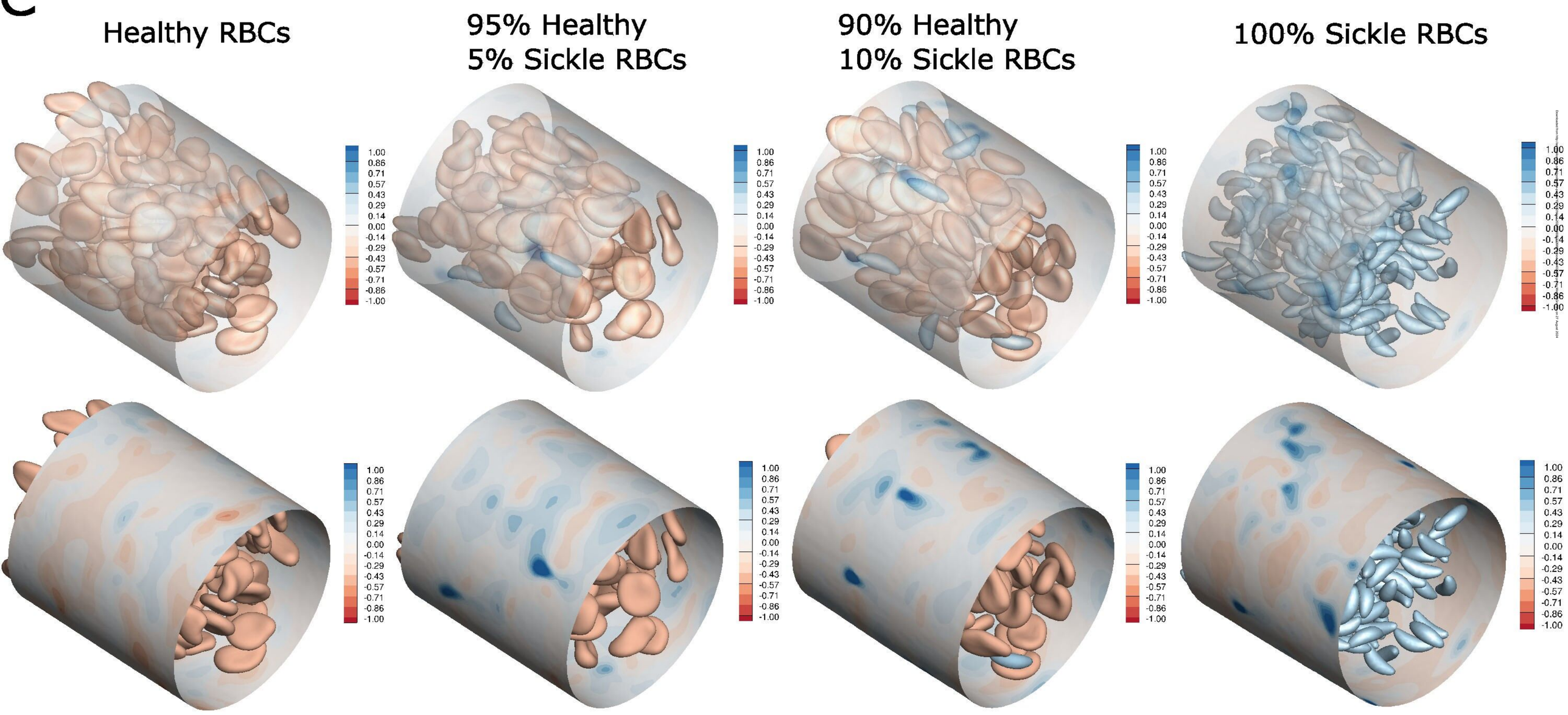

D

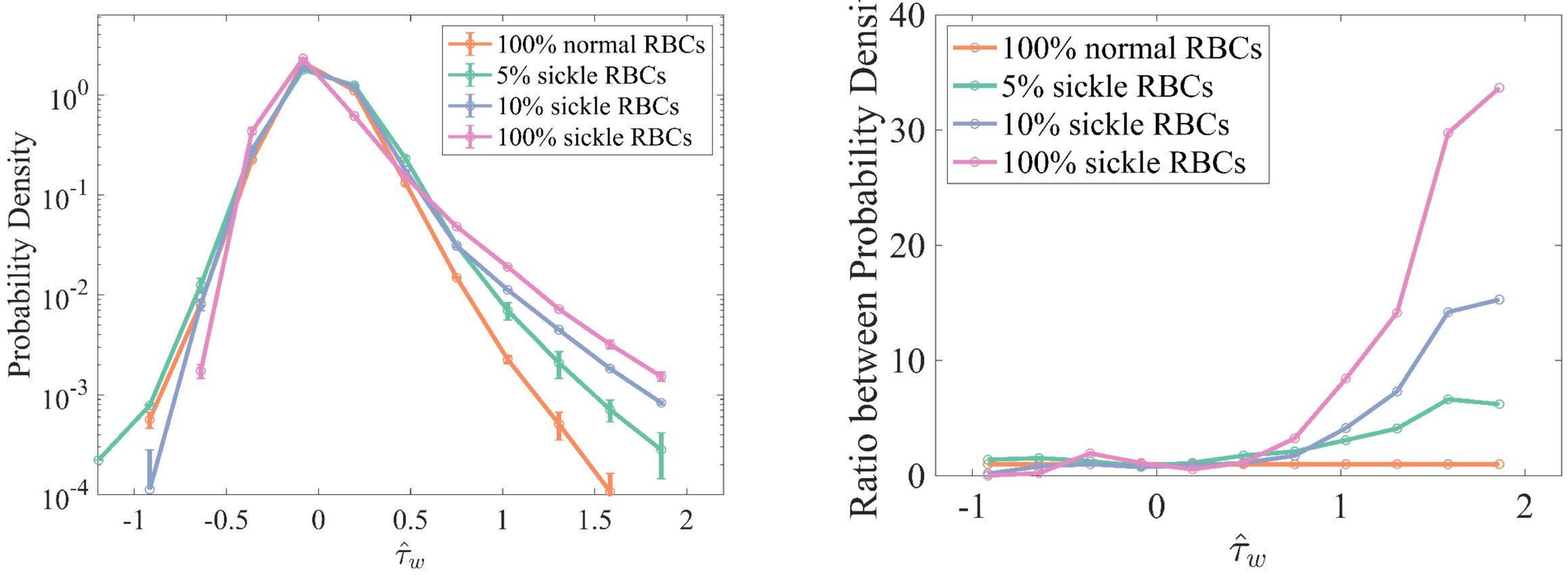

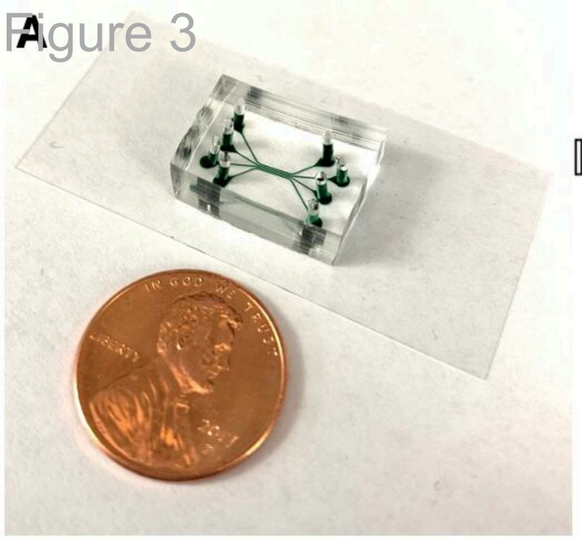

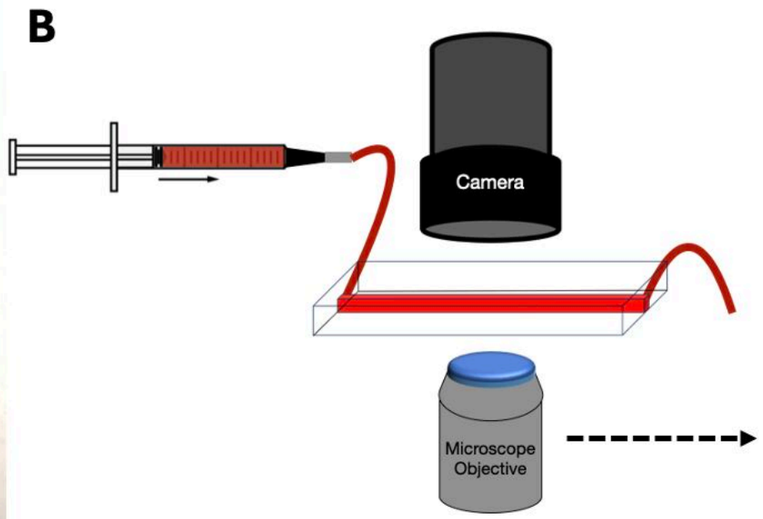

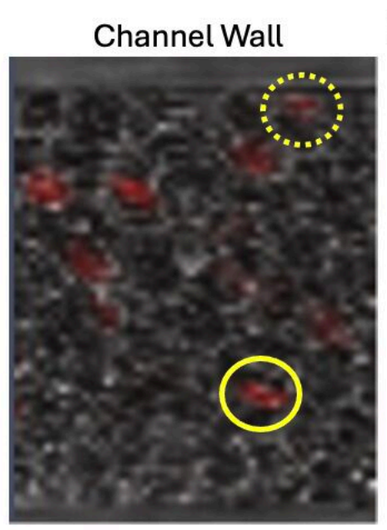

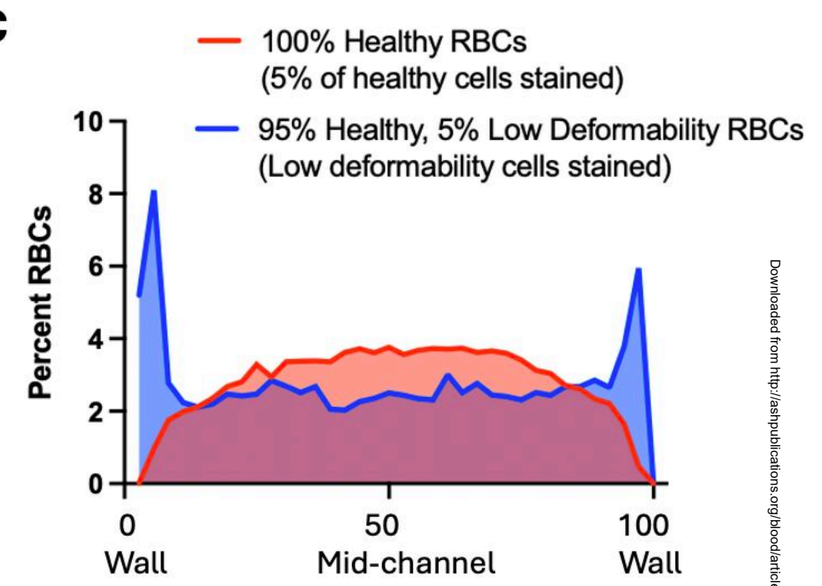

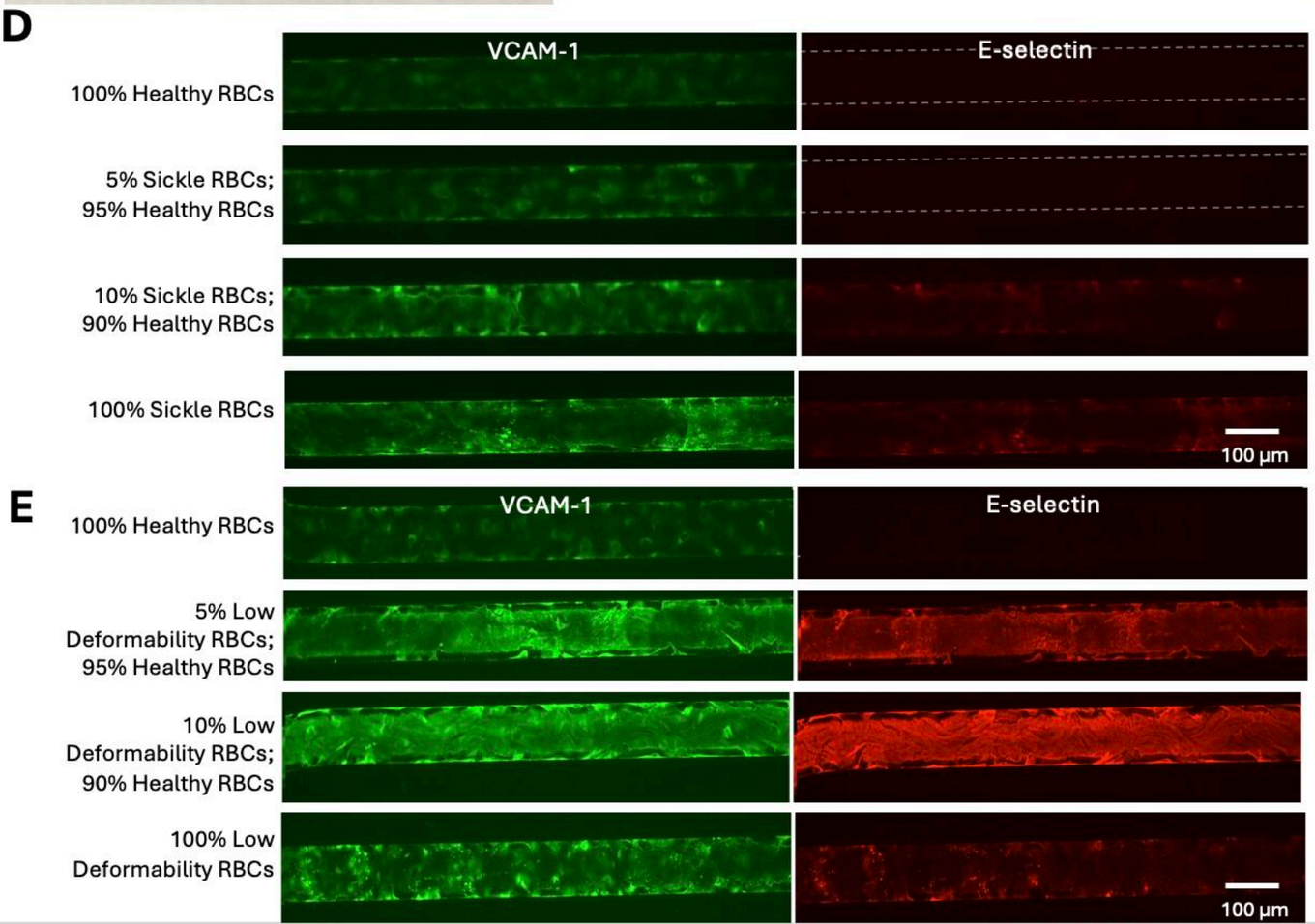

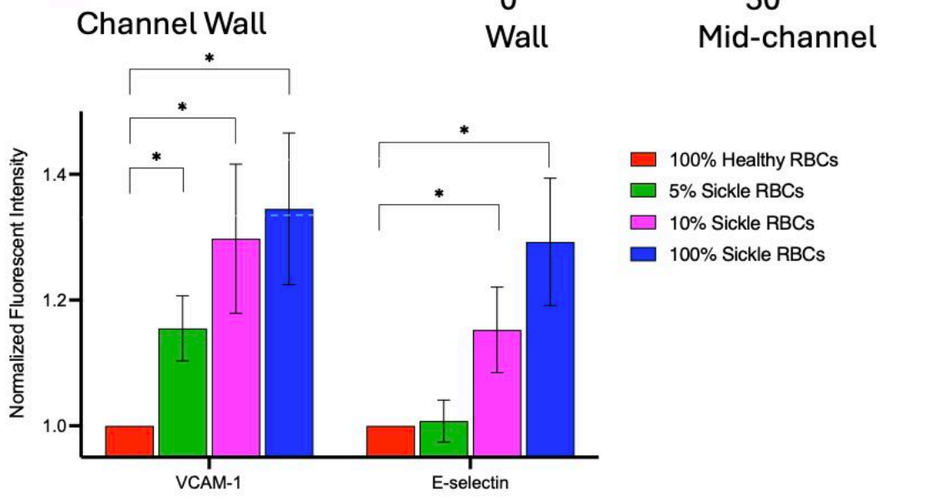

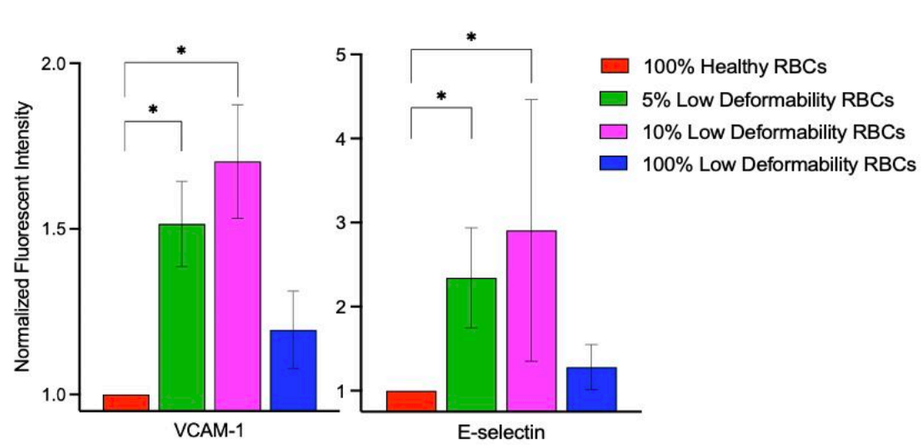

Figure 4

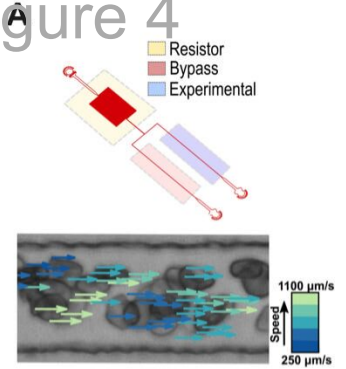

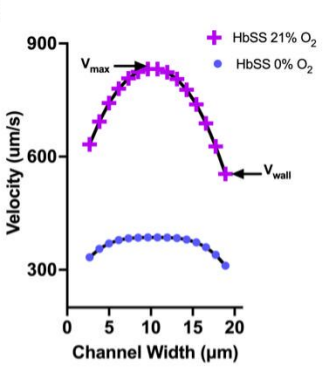

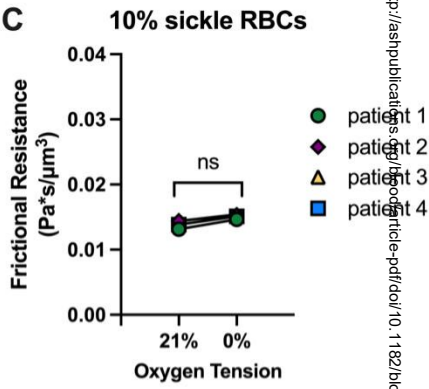

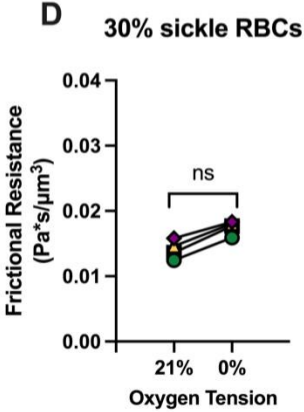

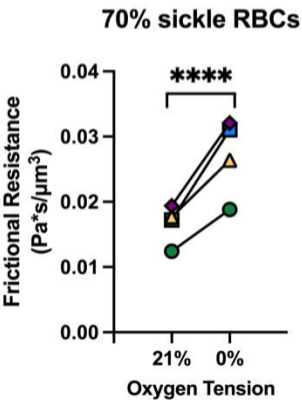

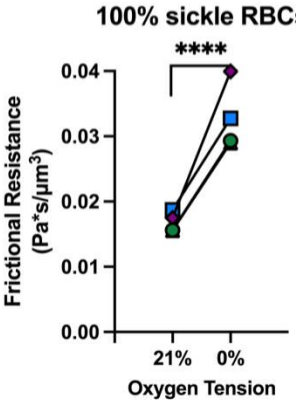

Figure 5

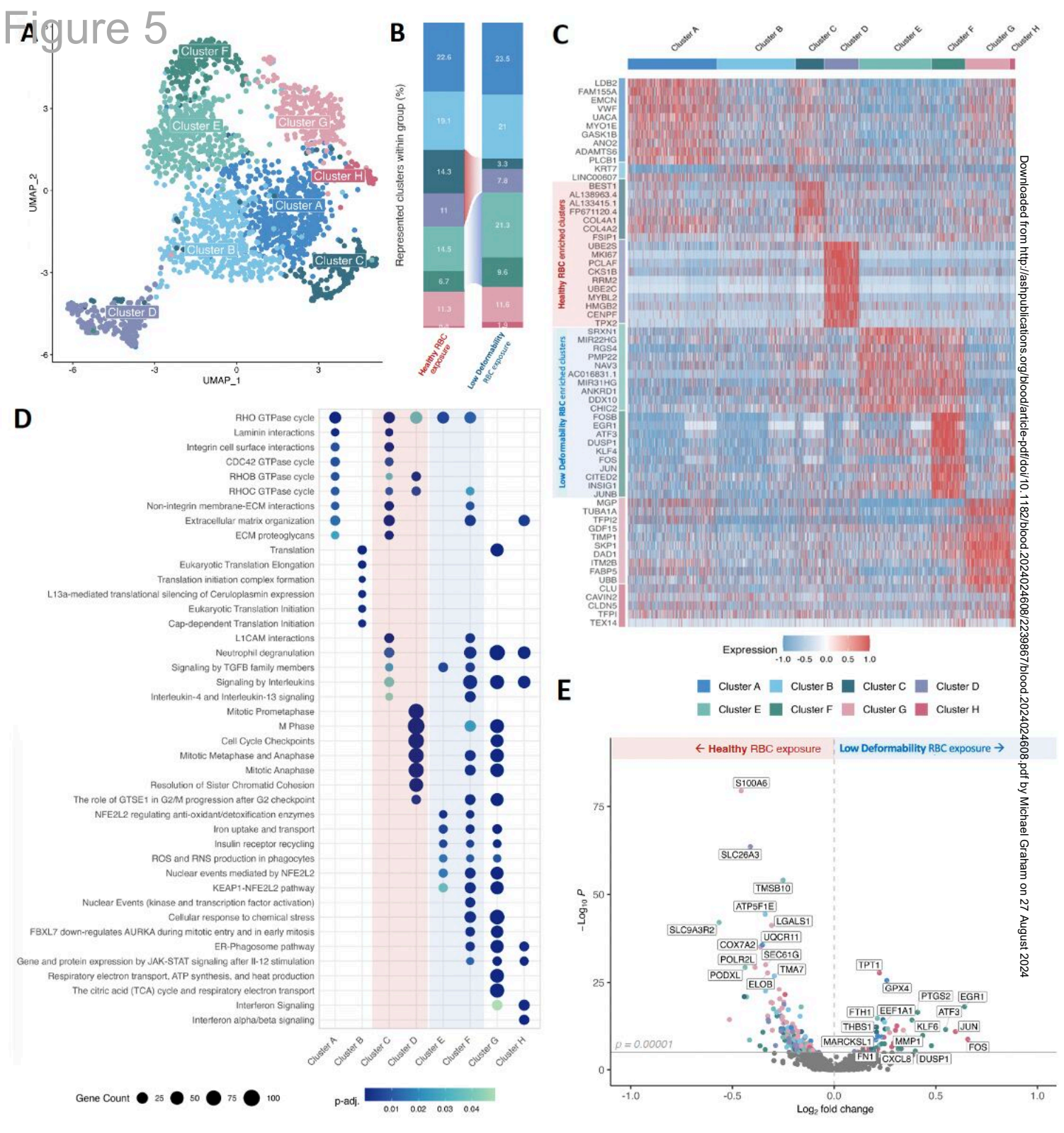

Figure 6

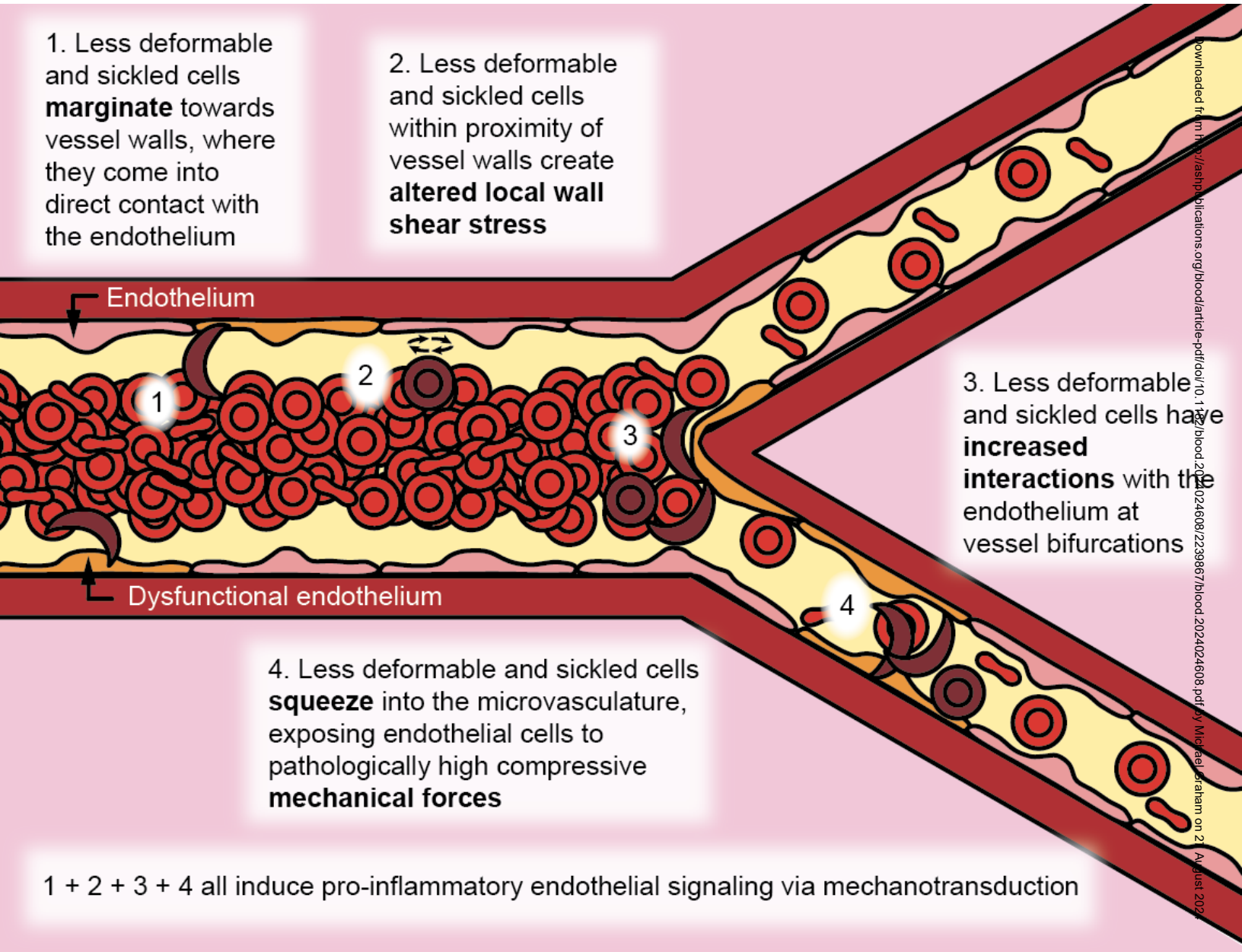

Role of Less Deformable Sickled Red Blood Cells on Endothelial Dysfunction

Context of Research

- Sickle cell disease (SCD) is canonically characterized by reduced red blood cell deformability leading to microvascular obstruction and inflammation
- This study ascertains how decreased red blood cell deformability in sickle cell disease may directly induce endothelial dysfunction

Methods

- Endothelialized microfluidic experiments
- Computational models of sickled red blood cells
- Microfluidic blood rheology deoxygenation experiments
- Single cell RNA sequencing

Main Findings

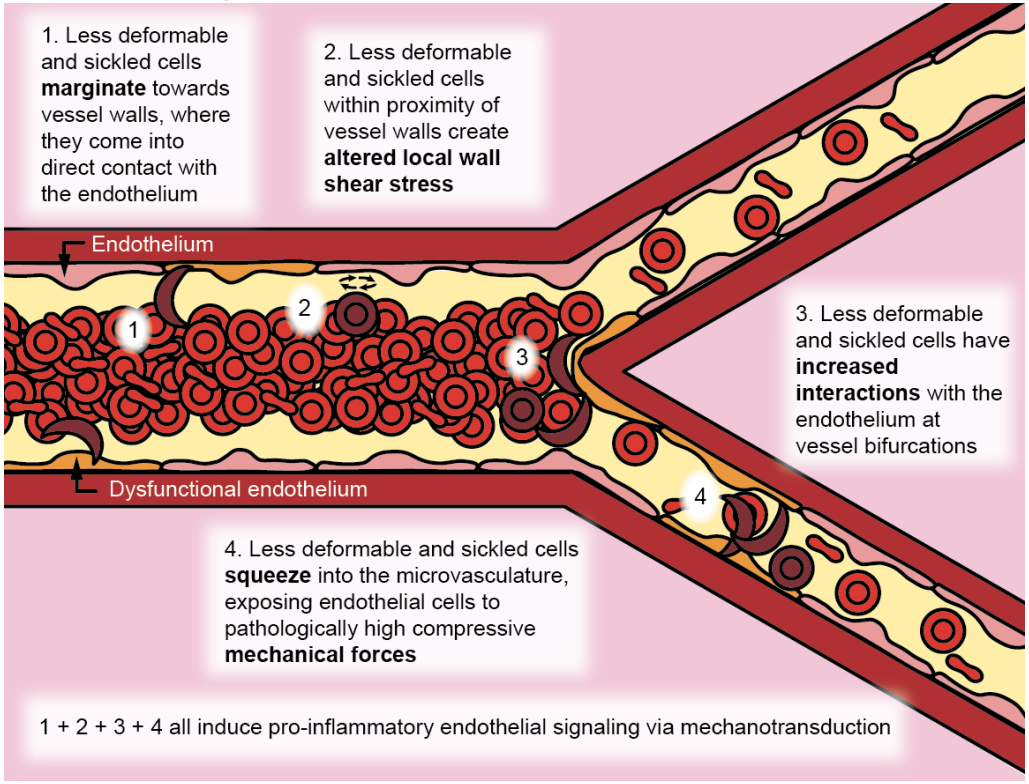

Conclusions: Less deformable sickle red blood cells marginate towards blood vessel walls leading to altered local wall shear stress and endothelial dysfunction. Additionally, pathological biophysical alterations in sickle red blood cells cause endothelial dysfunction independently from vaso-occlusion and adhesion.

*Caruso et al. DOI: 10.xxxx/**blood**.2024xxxxxx*

blood Visual Abstract